The Astronomical Journal, 129:630–646, 2005 February


# MULTICOLOR SURFACE PHOTOMETRY OF LENTICULAR GALAXIES. I. THE DATA

Sudhanshu Barway
School of Studies in Physics, Pandit Ravishankar Shukla University, Raipur 492010, India; ircrsu@sancharnet.in

Y. D. Mayya
Instituto Nacional de Astrofisíca, Óptica y Electrónica, Apdo. Postal 51 y 216, Luis Enrique Erro 1, 72000 Tonantzintla, Pue., Mexico; ydm@inaoep.mx

Ajit K. Kembhavi
Inter-University Centre for Astronomy and Astrophysics, Post Bag 4, Ganeshkhind, Pune 411007, India; akk@iucaa.ernet.in

and

S. K. Pandey[1]
School of Studies in Physics, Pandit Ravishankar Shukla University, Raipur 492010, India; ircrsu@sancharnet.in
*Received 2003 August 13; accepted 2004 October 20*

## ABSTRACT

We present multicolor surface and aperture photometry in the $B$, $V$, $R$, and $K'$ bands for a sample of 34 lenticular galaxies from the Uppsala General Catalogue. From surface photometric analysis, we obtain radial profiles of surface brightness, colors, ellipticity, position angle, and the Fourier coefficients that describe the departure of isophotal shapes from a purely elliptical form; we find the presence of dust lanes, patches, and ringlike structure in several galaxies in the sample. We obtain total integrated magnitudes and colors and find that these are in good agreement with the values from the Third Reference Catalogue. Isophotal colors are correlated with each other, following the sequence expected for early-type galaxies. The color gradients in lenticular galaxies are more negative than the corresponding gradients in elliptical galaxies. There is a good correlation between $B-V$ and $B-R$ color gradients, and the mean gradients in the $B-V$, $B-R$, and $V-K'$ colors are $-0.13 \pm 0.06$, $-0.18 \pm 0.06$, and $-0.25 \pm 0.11$ mag dex$^{-1}$ in radius, respectively.

*Key words:* galaxies: elliptical and lenticular, cD — galaxies: fundamental parameters — galaxies: photometry

## 1. INTRODUCTION

In 1936, Hubble introduced lenticular (S0) galaxies as a morphological transition class between elliptical and early-type spiral galaxies (Hubble 1958). The lenticular galaxies have disks with luminosity ranging from 10% to 100% of the bulge luminosity, but without any conspicuous spiral arms. From their appearance, and also their stellar content, they seem to be more like elliptical rather than spiral galaxies and have often been misclassified as a result of this fact.

It has been suggested (van den Bergh 1994) that there could be different, but overlapping, subpopulations among the lenticular galaxies. There are several scenarios possible for the formation of these galaxies. They could be of primordial origin or could have been formed by the stripping of gas from spirals, which changes the morphology (Abadi et al. 1999), or through the merger of unequal-mass spirals (Bekki 1998). There could be a significant difference in the ages of disks and bulges, in which case they should have different stellar populations, leading to different colors. Bothun & Gregg (1990) found that the bulges and disks of lenticular galaxies are well separated in the $B-H$ versus $J-K$ diagram, which they interpreted to mean that the disks are younger than the bulges by 3–5 Gyr. But Peletier & Balcells (1996) found that the color differences between the disks and bulges are much smaller than those found by Bothun & Gregg (1990) and inferred that the disks are only slightly younger than the bulges, with the difference in age being in the range 0–3 Gyr. In a study of 12 highly inclined lenticular galaxies, Michard & Poulain (2000) found that disks were often redder than bulges, which indicates that there could be a large concentration of dust in the disks. A detailed multiband study of the morphology of representative samples of lenticular galaxies, with possible separation of bulge and disk components, and comparison of their properties with those of elliptical galaxies and with the bulges and disks of spirals will be very important in addressing these and other possibilities.

We have observed a sample of 34 lenticular galaxies in the optical and infrared bands and present here their surface and aperture photometry, together with color profiles and mean color gradients. We will in a subsequent publication present a decomposition of the surface brightness distribution of the galaxies into bulge and disk components using the decomposition technique developed by Wadadekar et al. (1999). Using the results of the decomposition, it should be possible to see where the lenticular galaxies are situated relative to the fundamental plane of elliptical galaxies (see, e.g., Jørgensen et al. 1996 and references therein) and the photometric plane for elliptical galaxies and the bulges of spirals (Khosroshahi et al. 2000a, 2000b). With multiband data, it may be possible to determine in this manner the bulge-to-disk luminosity ratios of these galaxies in different bands, as well as the distribution of different colors as a function of distance from the center in the bulge and disk components separately, thus facilitating comparison with other galaxy types. Our data set will be very useful for detailed comparison with other galaxy types, as well as in constraining stellar population models for the lenticular galaxies.

The present paper deals with the details of the sample selection, observations, data reduction, and analysis. This paper is organized as follows: The selection criteria for the sample, details of the observations, and technique used in data reduction

[1] Visiting Associate, Inter-University Centre for Astronomy and Astrophysics (IUCAA).

TABLE 1

BASIC PARAMETERS OF THE SAMPLE GALAXIES

| UGC No. (1) | NGC No. (2) | *T*-Type (3) | Diameter (4) | $z$ (5) | $m_{ph}$ (6) | $M_B$ (7) |
|---|---|---|---|---|---|---|
| UGC 80 | NGC 16 | −3.0 | 1.8 × 1.0 | 0.010194 | 12.50 | −20.93 |
| UGC 491 | NGC 252 | −1.0 | 1.5 × 1.1 | 0.016645 | 13.40 | −21.65 |
| UGC 859 | NGC 473 | 0.0 | 1.7 × 1.1 | 0.007118 | 13.20 | −19.82 |
| UGC 926 | NGC 499 | −2.5 | 1.6 × 1.3 | 0.014673 | 13.00 | −21.55 |
| UGC 1250 | NGC 670 | −2.0 | 2.0 × 1.0 | 0.012352 | 13.10 | −20.76 |
| UGC 1823 | NGC 890 | −3.0 | 2.5 × 1.7 | 0.013323 | 12.50 | −22.31 |
| UGC 1964 | NGC 940 | −2.0 | 1.2 × 1.0 | 0.017319 | 13.40 | −21.64 |
| UGC 2039 | NGC 969 | −2.0 | 1.7 × 1.6 | 0.015054 | 13.50 | −21.51 |
| UGC 2187 | NGC 1040 | −2.0 | 1.7 × 0.8 | 0.016054 | 14.00 | −21.06 |
| UGC 2322 | NGC 1106 | −1.0 | 1.8 × 1.8 | 0.014467 | 13.70 | −21.39 |
| UGC 3087 | ... | −2.0 | 0.8 × 0.6 | 0.033010 | 14.20 | −22.28 |
| UGC 3178 | NGC 1671 | −2.0 | 1.1 × 0.9 | 0.021270 | 13.90 | −21.63 |
| UGC 3452 | NGC 2208 | −2.0 | 1.7 × 1.0 | 0.018763 | 14.00 | −21.26 |
| UGC 3536 | ... | −2.0 | 1.1 × 0.6 | 0.015641 | 14.40 | −20.86 |
| UGC 3567 | ... | −2.0 | 1.0 × 0.8 | 0.020164 | 14.20 | −21.26 |
| UGC 3642 | ... | −2.0 | 1.5 × 1.1 | 0.015004 | 13.50 | −21.47 |
| UGC 3683 | ... | −2.0 | 2.0 × 1.3 | 0.019076 | 14.10 | −21.53 |
| UGC 3699 | NGC 2332 | −2.0 | 1.5 × 1.0 | 0.019467 | 14.00 | −21.52 |
| UGC 3792 | ... | 0.0 | 1.8 × 1.3 | 0.020608 | 14.00 | −21.46 |
| UGC 3824 | ... | −2.0 | 0.9 × 0.8 | 0.017866 | 14.40 | −20.76 |
| UGC 4347 | NGC 2563 | −2.0 | 2.1 × 1.5 | 0.014944 | 13.70 | −21.06 |
| UGC 4767 | ... | −2.0 | 1.3 × 1.1 | 0.024127 | 14.00 | −21.80 |
| UGC 4901 | NGC 2804 | −2.0 | 2.2 × 2.0 | 0.028099 | 14.00 | −22.23 |
| UGC 5292 | NGC 3032 | −2.0 | 2.0 × 1.8 | 0.005114 | 13.00 | −19.43 |
| UGC 6013 | ... | −2.0 | 0.9 × 0.8 | 0.021898 | 13.90 | −21.69 |
| UGC 6389 | NGC 3648 | −2.0 | 1.3 × 0.8 | 0.006631 | 13.50 | −19.50 |
| UGC 6899 | NGC 3971 | −2.0 | 1.4 × 1.2 | 0.022489 | 13.90 | −21.75 |
| UGC 7142 | NGC 4143 | −2.0 | 2.3 × 1.4 | 0.003616 | 12.00 | −20.03 |
| UGC 7473 | NGC 4350 | −2.0 | 3.0 × 1.4 | 0.004140 | 11.50 | −20.48 |
| UGC 7880 | NGC 4638 | −3.0 | 2.2 × 1.4 | 0.003883 | 12.20 | −19.64 |
| UGC 7933 | NGC 4673 | −5.0 | 1.0 × 0.9 | 0.022856 | 13.70 | −21.99 |
| UGC 8675 | NGC 5273 | −2.0 | 2.8 × 2.5 | 0.003616 | 12.70 | −19.24 |
| UGC 9200 | NGC 5580 | −2.0 | 1.8 × 1.8 | 0.010814 | 13.60 | −20.46 |
| UGC 9592 | NGC 5784 | −2.0 | 1.9 × 1.8 | 0.017912 | 13.70 | −21.78 |
| UGC 11178 | NGC 6599 | −2.0 | 1.3 × 1.2 | 0.010120 | 13.70 | −20.30 |
| UGC 11356 | NGC 6703 | −2.5 | 2.5 × 2.3 | 0.008209 | 12.40 | −21.14 |
| UGC 11781 | ... | −2.0 | 1.4 × 1.1 | 0.015501 | 13.70 | −21.74 |
| UGC 11972 | NGC 7248 | −2.5 | 1.7 × 0.9 | 0.014627 | 13.60 | −21.22 |
| UGC 12443 | NGC 7539 | −2.0 | 1.5 × 1.2 | 0.020174 | 13.70 | −21.88 |
| UGC 12655 | ... | −2.0 | 1.4 × 0.9 | 0.017269 | 14.00 | −21.24 |

NOTE.—Cols. (1) and (2) give the UGC and NGC number, respectively, col. (3) gives the morphological type from the RC3, cols. (4) and (5) give the diameter (in arcminutes) along the major and minor axes, respectively, and the redshift from NED, col. (6) gives the photographic magnitude from the UGC, and col. (7) gives the absolute $B$ magnitude for $H_0 = 50$ km s$^{-1}$ Mpc$^{-1}$.

are described in § 2. The analysis and results from the surface photometry and aperture photometry are discussed in § 3. The distribution of color gradients is discussed in § 4, and a summary of the results is presented in § 5. An appendix contains comments on individual galaxies.

## 2. OBSERVATIONS AND DATA REDUCTION

### 2.1. *The Sample*

Our sample consists of 40 bright and medium-sized galaxies, classified as lenticular, from the Uppsala General Catalogue of Galaxies (UGC; Nilson 1973). The UGC is essentially complete to a limiting major-axis diameter of 1′, or to a limiting apparent magnitude of 14.5 on the blue prints of the Palomar Observatory Sky Survey. Coverage is limited to the sky north of declination −2°.5. For our sample we selected galaxies with apparent blue magnitude brighter than $m_B = 14$, diameter $D_{25} < 3'$, and declination in the range $5^\circ < \delta < 64^\circ$. The sample galaxies are listed in Table 1. Our sample, though not complete, is representative of lenticular galaxies in the field with the above properties.

### 2.2. *Optical Imaging*

Our optical *BVR*-band observations were carried out with the 2.1 m telescope of the Observatorio Astrofísico Guillermo Haro (OAGH) in Cananea, Mexico. We used a Tektronix CCD of 1024 × 1024 pixel format at the f/12 Cassegrain focus of the telescope with 3 × 3 pixel binning, resulting in a scale of 0″.6 pixel$^{-1}$ and a field of view of 3′.4 × 3′.4. Typically, two exposures each of 10, 5, and 5 minutes in *B*, *V*, and *R* respectively were taken for each galaxy. Exposure times were reduced if the central pixels were close to saturation. Twilight sky exposures were taken for

TABLE 2
Log of Observations

| Galaxy | Date of Observation | | Exposure Time (s) | | | | Seeing FWHM (arcsec) | | | |
|---|---|---|---|---|---|---|---|---|---|---|
| | *BVR* | $K'$ | *B* | *V* | *R* | $K'$ | *B* | *V* | *R* | $K'$ |
| UGC 80 | 2002 Oct 4 | 2001 Oct 10 | 1200 | 360 | 540 | 750 | 2.24 | 2.07 | 2.03 | 1.56 |
| UGC 491 | 2002 Oct 5 | 2001 Oct 12 | 1200 | 600 | 600 | 750 | 1.85 | 2.18 | 2.18 | 1.52 |
| UGC 859 | 2001 Dec 14 | 2001 Oct 9 | 1200 | 600 | 600 | 900 | 2.41 | 2.81 | 2.64 | 1.76 |
| UGC 926 | 2002 Oct 5 | 2001 Oct 10 | 1200 | 360 | 540 | 750 | 1.80 | 1.66 | 1.78 | 1.49 |
| UGC 1250 | 2002 Oct 4 | 2001 Oct 10 | 1200 | 600 | 600 | 900 | 2.31 | 2.10 | 2.01 | 1.48 |
| UGC 1823 | 2001 Dec 14 | 2001 Oct 9 | 1200 | 600 | 600 | 750 | 2.43 | 2.78 | 2.67 | 1.61 |
| UGC 1964 | 2001 Dec 14 | 2001 Oct 9 | 1200 | 600 | 600 | 900 | 2.10 | 2.09 | 2.18 | 1.60 |
| UGC 2039 | 2002 Oct 5 | 2001 Oct 12 | 1200 | 600 | 600 | 600 | 1.91 | 2.11 | 2.01 | 1.64 |
| UGC 2187 | ... | 2001 Oct 10 | ... | ... | ... | 900 | ... | ... | ... | 1.47 |
| UGC 2322 | ... | 2001 Oct 9 | ... | ... | ... | 780 | ... | ... | ... | 1.49 |
| UGC 3087 | 2002 Feb 8 | 2002 Mar 24 | 1200 | 540 | 540 | 480 | 2.16 | 1.98 | 2.14 | 2.06 |
| UGC 3178 | 2002 Feb 9 | 2002 Mar 23 | 1200 | 600 | 600 | 320 | 2.02 | 1.87 | 1.87 | 1.75 |
| UGC 3452 | 2001 Dec 14 | 2000 Dec 16 | 1200 | 600 | 600 | 600 | 2.55 | 2.76 | 2.63 | 1.58 |
| UGC 3536 | 2002 Feb 8 | 2002 Mar 26 | 1200 | 540 | 540 | 105 | 2.14 | 2.01 | 2.05 | 1.54 |
| UGC 3567 | 2002 Feb 7 | 2002 Feb 28 | 1200 | 600 | 600 | 750 | 2.17 | 1.97 | 2.04 | 1.92 |
| UGC 3642 | 2002 Feb 9 | 2002 Feb 26 | 1200 | 720 | 720 | 750 | 1.86 | 2.04 | 1.90 | 1.48 |
| UGC 3683 | 2002 Feb 8 | 2002 Mar 23 | 1200 | 600 | 600 | 750 | 2.26 | 2.26 | 1.97 | 2.07 |
| UGC 3699 | 2002 Oct 5 | 2001 Oct 12 | 600 | 360 | 540 | 750 | 2.58 | 2.58 | 2.59 | 1.89 |
| UGC 3792 | 2001 Dec 14 | 2001 Oct 10 | 1200 | 600 | 600 | 750 | 2.28 | 2.69 | 2.43 | 1.85 |
| UGC 3824 | 2002 Feb 7 | 2002 Mar 26 | 1800 | 600 | 600 | 105 | 2.13 | 2.13 | 2.24 | 1.66 |
| UGC 4347 | 2001 Dec 14 | 2001 Mar 8 | 1200 | 600 | 600 | 540 | 2.51 | 2.71 | 2.55 | 1.88 |
| UGC 4767 | 2002 Feb 8 | 2002 Mar 24 | 1200 | 600 | 600 | 600 | 2.42 | 2.07 | 2.08 | 1.92 |
| UGC 4901 | 2002 Feb 9 | 2002 Mar 26 | ... | 600 | 600 | 105 | ... | 1.75 | 1.85 | 1.45 |
| UGC 5292 | ... | 2001 Jun 7 | ... | ... | ... | 900 | ... | ... | ... | 1.67 |
| UGC 6013 | 2002 Feb 7 | 2001 Feb 8 | ... | 600 | 600 | 840 | ... | 2.50 | 2.07 | 1.64 |
| UGC 6389 | 2002 Feb 8 | 2002 Mar 23 | 1200 | 540 | 540 | 700 | 1.92 | 2.05 | 2.03 | 1.89 |
| UGC 6899 | 2002 Feb 8 | 2002 Mar 23 | 1200 | 600 | 600 | 840 | 1.96 | 1.97 | 1.94 | 1.27 |
| UGC 7142 | ... | 2002 Mar 23 | ... | ... | ... | 450 | ... | ... | ... | 2.07 |
| UGC 7473 | 2002 Feb 9 | 2002 Mar 22 | 900 | 450 | 270 | 260 | 2.12 | 2.13 | 2.08 | 1.43 |
| UGC 7880 | 2002 Feb 9 | 2002 Mar 25 | 1200 | 270 | 600 | 500 | 2.37 | 2.64 | 2.41 | 1.79 |
| UGC 7933 | 2002 Feb 7 | 2002 Mar 8 | ... | 540 | 540 | 840 | ... | 2.47 | 2.26 | 1.79 |
| UGC 8675 | 2002 Feb 8 | 2002 Mar 22 | 1200 | 600 | 540 | 310 | 2.04 | 1.91 | 1.82 | 1.63 |
| UGC 9200 | ... | 2001 Mar 7 | ... | ... | ... | 840 | ... | ... | ... | 1.50 |
| UGC 9592 | ... | 2002 Mar 24 | ... | ... | ... | 600 | ... | ... | ... | 1.92 |
| UGC 11178 | 2002 Oct 4 | 2002 Mar 22 | 900 | 600 | 600 | 240 | 2.15 | 2.06 | 2.20 | 1.39 |
| UGC 11356 | 2002 Oct 5 | 2002 Mar 23 | 1200 | 240 | 360 | 420 | 1.91 | 1.91 | 1.91 | 1.80 |
| UGC 11781 | 2002 Oct 4 | 2001 Oct 9 | 900 | 600 | 600 | 540 | 1.99 | 1.94 | 2.07 | 1.83 |
| UGC 11972 | 2002 Oct 5 | 2001 Oct 10 | 900 | 540 | 360 | 900 | 2.07 | 1.79 | 1.78 | 1.50 |
| UGC 12443 | 2001 Dec 14 | 2001 Oct 12 | 1200 | 600 | 600 | 900 | 2.87 | 2.89 | 2.92 | 1.56 |
| UGC 12655 | 2002 Oct 4 | 2001 Oct 9 | 1200 | 600 | 600 | 120 | 2.24 | 1.98 | 2.12 | 1.59 |

flat-fielding purposes. Several bias frames were obtained at the start and end of each night. All the observations were carried out over three runs in 2001 December, 2002 February, and 2002 October. A total of 34 galaxies were observed in the optical bands. For the galaxies UGC 1964, 3178, 4901, 6013, and 7933 from the observed set, the quality of the images was not good enough for photometric analysis. Table 2 contains a detailed log of the observations.

### 2.3. *Near-Infrared Imaging*

We obtained images of all 40 sample galaxies in the near-infrared $K'$ band with the 2.1 m telescope of the Observatorio Astronómico Nacional in San Pedro Mártir, Mexico (SPM). The CAMILA instrument (Cruz-González et al. 1994), which hosts a $256 \times 256$ pixel NICMOS3 detector, was used in imaging mode with the f/4.5 focal reducer configuration in all our observations. This results in a spatial resolution of $0\farcs85$ pixel$^{-1}$ and a total field of view of $3\farcm6 \times 3\farcm6$. Each $K'$ observation consisted of a sequence of object and sky exposures, with the integration time of an individual exposure limited by the sky counts (or in some cases the nucleus), which were kept well below the nonlinear regime of the detector. A typical $K'$ image sequence consisted of 10 exposures, six on the object and four on the sky. The net exposure times were typically 10 minutes. A series of twilight and night-sky images were taken for flat-fielding purposes. The $K'$ observations were carried out over four runs in 2000 December, 2001 March, 2001 October, and 2002 March.

The sky conditions for both optical and near-infrared observations were generally photometric, and the seeing FWHM was in the range $1\farcs5$–$2\farcs5$ on different nights. The average sky brightness was 21.14, 20.72, 20.18, and 12.27 mag arcsec$^{-2}$ in the *B*, *V*, *R*, and $K'$ bands, respectively. The sky brightness in $K'$ also includes the background emitted by the warm optics.

### 2.4. *Data Reduction*

The basic data reduction for both the optical and near-infrared $K'$ images involved subtraction of the bias and sky

frames, division by flat-field frames, registration of the images to a common coordinate system, and then stacking of all the images of a given galaxy in each filter. Night-to-night variations of the optical bias frames were negligible, and hence bias frames of an entire run were stacked together using the median algorithm to form a master bias frame, which was then subtracted from all the other frames. Preparation of the optical flat fields followed the conventional technique, wherein bias-subtracted flats were stacked and the resultant frame was normalized to its mean value to form a master flat in each filter. Bias-subtracted images of the program galaxies were divided by the normalized flat field in the corresponding filter. The optical images suffered from a stray-light problem that resulted in a gradient in the sky background, which roughly ran through one of the diagonals of the CCD chip. The gradient was found to be stable throughout each run and the mean counts scaled linearly with exposure time. After several experiments, we found that the best way to get rid of the gradient was to subtract a mean blank-sky image from the data images. For this purpose, special blank fields were observed in each filter with exposure times matching the typical exposure times of the object frames. In the 2001 December run, three blank-sky frames were used in each filter to prepare a median gradient image, while in the 2002 February run six frames were used. The adopted procedure eliminated any gradient from the sky background.

For the $K'$ images, a bias frame taken immediately before an object exposure was subtracted as part of the data acquisition. A master $K'$ flat field for each night of observing was prepared as follows: The night-sky flats were first stacked and then subtracted from stacked twilight flats. The frames obtained in this fashion for each run were then combined and normalized to the mean value of the resultant frame to form a master $K'$ flat. The sky frames of each sequence of observations were combined, and the resultant image was subtracted from each of the object frames to obtain a sky-subtracted image. Flat-fielding was done by dividing the sky-subtracted images of the object by the normalized master flat. The resulting images were aligned to a common coordinate system using common stars in the frames and then combined using the median operation. Only good images (as defined in the CAMILA manual; see Cruz-González et al. 1994) were used in the $K'$ combination. The resulting combined $K'$ images were aligned to corresponding images from the Digitized Sky Survey. As a final step in the reduction procedure, the mutually aligned optical images were aligned to the $K'$-image coordinate system. The transformed star positions in the images agreed to within $0\farcs2$ as judged from the coordinates of common stars.

All image reductions were carried out using the Image Reduction and Analysis Facility (IRAF)[2] and the Space Telescope Science Data Analysis System (STSDAS). The IRAF external package COLOR was used to make color composite images, by combining images taken in three different bands, *B*, *V*, and *R* or *V*, *R*, and $K'$. Gray-scale versions of these color composite images are shown in Figure 1, where north is up and east is to the left.

### 2.5. *Photometric Calibration*

Dipper-asterism stars in the M67 field were observed in order to enable accurate photometric calibration of our optical observations. The stars in this field span a wide color range ($-0.05 < B-V < 1.35$), which includes the range of colors of the program galaxies, and hence are suitable for obtaining the transformation coefficients to the Cousins *BVR* system defined by Bessell (1990). The transformation equations are

$$B = b_0 + \alpha_B + \beta_B(b_0 - v_0), \quad (1)$$

$$V = v_0 + \alpha_V + \beta_V(b_0 - v_0), \quad (2)$$

$$R = r_0 + \alpha_R + \beta_R(v_0 - r_0), \quad (3)$$

where *B*, *V*, and *R* are standard magnitudes, $b_0$, $v_0$, and $r_0$ are extinction-corrected instrumental magnitudes, $\alpha_B$, $\alpha_V$, and $\alpha_R$ are the zero points, and $\beta_B$, $\beta_V$, and $\beta_R$ are the color coefficients in the *B*, *V*, and *R* bands, respectively. Typical extinction coefficients for the observatory (0.20, 0.11, and 0.07 for *B*, *V*, and *R*, respectively) were used. Considering that the objects and the standard stars were observed as close to the meridian as possible, and that in none of the cases did the air mass exceed 1.3, the error introduced due to possible variation in the extinction coefficients is less than 0.02 mag. The coefficients $\alpha$ and $\beta$ were obtained by using the *BVR* standard magnitudes of Chevalier & Ilovaisky (1991). Resulting values of $\alpha$ and $\beta$ are given in Table 3. The relatively large color coefficient on the *R*-band calibration is due to the nonstandard nature of the filter used in the observations. The stability of the $\alpha$ on a given night was checked using at least two other standard fields from the Landolt Selected Areas (Landolt 1992). The standard fields observed during our runs were SA 110-232, PG 2336+004, Rubin 149, and PG 1323−086. Overall, the zero points within a single night agreed to within 0.02 mag. Night-to-night variation of the zero point was also within 0.02 mag.

The detector and filter system combination that we used for the near-infrared observations is identical to that used in the observations of standards by Hunt et al. (1998), and hence the color coefficients are expected to be negligibly small. We verified this by observing fields AS 17 and AS 36, which contain stars spanning a wide range of colors. We observed at least two standard fields each night, each field containing more than one star and some fields, such as AS 17, containing five stars. The $K'$-band zero point was obtained for each night as the mean of zero points from different stars, and the average value is $\alpha_{K'} = 20.15 \pm 0.05$.

For reddening corrections due to Galactic extinction, we adopt the values given by Schlegel et al. (1998) for each filter in the optical range. For near-infrared observations we use the extinction law given by Rieke & Lebofsky (1985). When galaxies at different redshifts are seen through a fixed passband, the collected light comes from different wavelength ranges in the rest frame of the respective galaxies. *K*-correction is used to transform the rest-frame magnitudes of each object to the passband of the filter. We have used an approximate form of the *K*-correction, applicable for small *z*, from Persson et al. (1979), Frei & Gunn (1994), and Fukugita et al. (1995). For the four filters we have $K_B = 4.4z$, $K_V = 3.24z$, $K_R = 2.12z$, and $K_{K'} = -3z$, respectively, where *z* is the redshift of the galaxy. We have listed the combination of Galactic extinction and *K*-correction for individual galaxies in Table 4.

## 3. ANALYSIS

### 3.1. *Sky Background*

An accurate estimation of the sky background is a crucial step in surface photometric analysis, as even small uncertainties

[2] IRAF is distributed by the National Optical Astronomy Observatory, which is operated by the Association of Universities for Research in Astronomy, Inc., under cooperative agreement with the National Science Foundation.

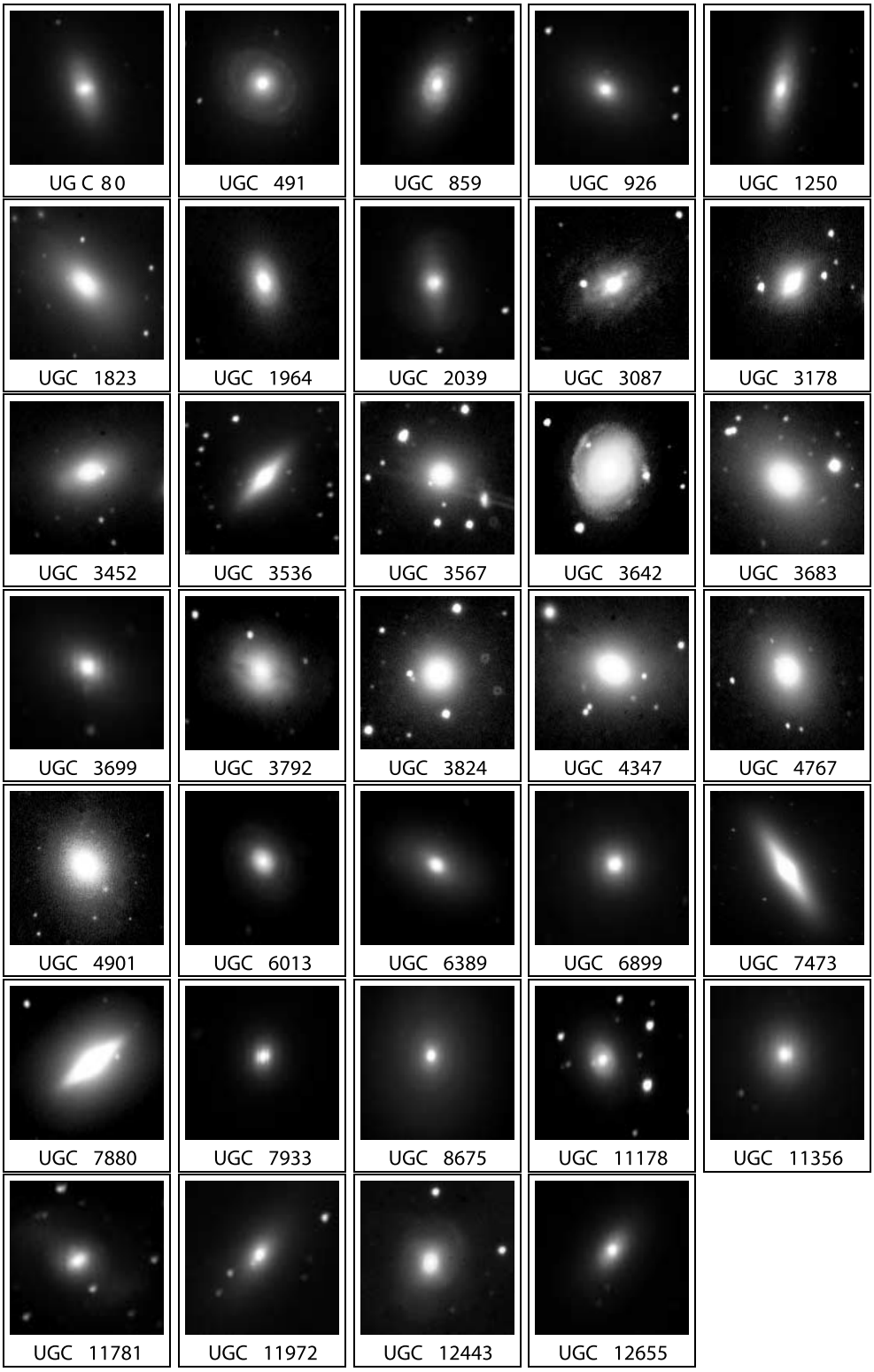


FIG. 1.—Gray-scale representations of the color composite images of our sample galaxies (see § 2.4).

in determining the sky can lead to significant errors in the estimation of the galaxy surface brightness and color profiles, especially where the surface brightness becomes comparable to or less than the sky brightness. In those cases in which the galaxy image is small enough that the frame contains portions of the sky unaffected by the galaxy, it is possible to estimate the sky using the "boxes method" (see Peletier et al. 1990a), where the background is estimated from a series of boxes chosen to avoid the sample galaxy, foreground stars, and any other contaminating objects that may be present. We have used 20 boxes of size $5 \times 5$ pixels near the corners of the CCD frame and have adopted the mean of the median count in these boxes as the sky background. The rms dispersion over the mean of 20 boxes is found to be 0.6% of the mean in the $B$, $V$, and $R$ bands and 0.2% of the mean in the $K'$ band. When a galaxy is so large that the whole frame is affected by it, use of the boxes method leads to

TABLE 3
Zero Points and Transformation Coefficients for Optical Observations

| Filter | Zero Point, $\alpha$ | Color Coefficient, $\beta$ |
|---|---|---|
| 2002 Feb: | | |
| *B* | 22.88 ± 0.03 | −0.095 ± 0.016 |
| *V* | 23.49 ± 0.02 | +0.075 ± 0.010 |
| *R* | 22.45 ± 0.05 | −0.408 ± 0.081 |
| 2002 Oct: | | |
| *B* | 22.60 ± 0.03 | −0.095 ± 0.016 |
| *V* | 23.21 ± 0.04 | +0.075 ± 0.010 |
| *R* | 22.15 ± 0.03 | −0.408 ± 0.081 |

overestimation of the background. In such cases, the background can be determined by fitting a power law of the form $I(r) = \text{sky} + I(0)r^{-\alpha}$ to the outer parts of the surface brightness profile. Following Jørgensen et al. (1992) and Goudfrooij et al. (1994), we fit the function to the region of the profile with $r > 50''$ typically, separately for $\alpha = 2$ and $\alpha = 3$, and use the mean of the respective best-fit constant values as the background. The error in the sky background estimation is taken to be half the difference of the sky values obtained for the two fits. We have used both techniques for all galaxies in our sample, and we find that in most cases the two methods agree within ∼0.005 mag (i.e., 1 $\sigma$ difference), because of the small size of the galaxies relative to the CCD frame. In the case of the galaxies UGC 4347, 7473, 7880, 8675, and 11356, which cover most of the frame, the power-law fit provides a background that is ∼0.06 mag (i.e., 10 $\sigma$ difference) fainter than the boxes method, and we adopt the former as the background estimation. In the $K'$-band images, the background is already subtracted from the many individual frames for each galaxy during the preprocessing stage (see § 2.4). However, to check for any residual background that may be present in processed frames used in the analysis, we have again applied the two techniques for the background estimation. We find that the two estimates agree very well (∼0.0006 mag, except in two cases where the agreement is within ∼0.001 mag).

### 3.2. *Surface Photometry: Isophotal Analysis*

We have fitted ellipses to the isophotes in our *B*-, *V*-, *R*-, and $K'$-band images, using the task ELLIPSE in the STSDAS package available in IRAF. The fitting algorithm used is described in detail by Jedrzejewski (1987) and uses the intensity distribution along a trial ellipse, which can be expressed as a Fourier series

$$I(\phi) = I_0 + \sum_n a_n \sin n\phi + \sum_n b_n \cos n\phi, \qquad (4)$$

where $\phi$ is the ellipse eccentric anomaly, $I_0$ is the mean intensity along the ellipse, and $a_n$ and $b_n$ are harmonic amplitudes.

The fitting was started a few arcseconds from the center of the galaxy image to minimize the effects of seeing and stopped at the isophotes where the mean counts become comparable to

TABLE 4
Integrated Magnitudes and Colors

| | | | | | Galactic Extinction + *K*-Correction | | | |
|---|---|---|---|---|---|---|---|---|
| Galaxy (1) | *B* (2) | *B*−*V* (3) | *B*−*R* (4) | *V*−*K*′ (5) | *B* (6) | *B*−*V* (7) | *B*−*R* (8) | *V*−*K*′ (9) |
| UGC 80 | 13.01 ± 0.04 | 0.95 ± 0.01 | 1.54 ± 0.01 | 3.34 ± 0.04 | 0.25 | 0.06 | 0.10 | 0.20 |
| UGC 491 | 13.46 ± 0.05 | 0.97 ± 0.02 | 1.61 ± 0.01 | 3.36 ± 0.05 | 0.32 | 0.07 | 0.13 | 0.27 |
| UGC 859 | 13.41 ± 0.03 | 0.78 ± 0.01 | 1.28 ± 0.01 | 3.22 ± 0.06 | 0.41 | 0.09 | 0.16 | 0.30 |
| UGC 926 | 13.32 ± 0.05 | 1.02 ± 0.01 | 1.66 ± 0.01 | 3.59 ± 0.03 | 0.36 | 0.08 | 0.14 | 0.29 |
| UGC 1250 | 13.53 ± 0.03 | 0.81 ± 0.01 | 1.37 ± 0.01 | 3.32 ± 0.04 | 0.36 | 0.08 | 0.14 | 0.29 |
| UGC 1823 | 12.58 ± 0.03 | 0.96 ± 0.01 | 1.53 ± 0.01 | 3.37 ± 0.04 | 0.39 | 0.09 | 0.15 | 0.31 |
| UGC 2039 | 13.38 ± 0.08 | 0.97 ± 0.02 | 1.59 ± 0.02 | 3.48 ± 0.05 | 0.57 | 0.13 | 0.22 | 0.44 |
| UGC 3087 | 14.60 ± 0.07 | 0.62 ± 0.05 | 1.09 ± 0.05 | 3.72 ± 0.18 | 0.42 | 0.10 | 0.17 | 0.35 |
| UGC 3452 | 13.70 ± 0.07 | 1.09 ± 0.01 | 1.69 ± 0.01 | 3.69 ± 0.04 | 0.74 | 0.17 | 0.29 | 0.56 |
| UGC 3536 | 13.39 ± 0.09 | 1.02 ± 0.01 | 1.60 ± 0.01 | 3.62 ± 0.03 | 0.54 | 0.12 | 0.21 | 0.42 |
| UGC 3567 | 14.36 ± 0.06 | 1.03 ± 0.01 | 1.61 ± 0.01 | 3.54 ± 0.05 | 0.44 | 0.10 | 0.18 | 0.36 |
| UGC 3642 | 13.51 ± 0.05 | 0.91 ± 0.02 | 1.50 ± 0.02 | 3.39 ± 0.07 | 0.26 | 0.06 | 0.11 | 0.23 |
| UGC 3683 | 13.72 ± 0.06 | 1.04 ± 0.01 | 1.64 ± 0.01 | 3.76 ± 0.04 | 0.48 | 0.11 | 0.19 | 0.39 |
| UGC 3699 | 14.13 ± 0.12 | 1.08 ± 0.01 | 1.71 ± 0.01 | 3.64 ± 0.02 | 0.45 | 0.10 | 0.18 | 0.37 |
| UGC 3792 | 14.07 ± 0.05 | 1.10 ± 0.01 | 1.75 ± 0.01 | 3.57 ± 0.05 | 0.38 | 0.09 | 0.15 | 0.32 |
| UGC 3824 | 14.22 ± 0.05 | 0.99 ± 0.01 | 1.57 ± 0.01 | 3.30 ± 0.05 | 0.31 | 0.07 | 0.13 | 0.27 |
| UGC 4347 | 13.40 ± 0.04 | 1.01 ± 0.01 | 1.57 ± 0.01 | 3.57 ± 0.04 | 0.25 | 0.06 | 0.10 | 0.22 |
| UGC 4767 | 14.26 ± 0.05 | 0.99 ± 0.01 | 1.53 ± 0.01 | 3.55 ± 0.05 | 0.19 | 0.04 | 0.08 | 0.21 |
| UGC 6389 | 13.57 ± 0.03 | 0.93 ± 0.01 | 1.45 ± 0.01 | 3.35 ± 0.05 | 0.11 | 0.02 | 0.04 | 0.10 |
| UGC 6899 | 14.01 ± 0.04 | 0.88 ± 0.01 | 1.42 ± 0.01 | 3.37 ± 0.06 | 0.17 | 0.04 | 0.08 | 0.19 |
| UGC 7473 | 12.01 ± 0.02 | 0.93 ± 0.01 | 1.46 ± 0.01 | 3.39 ± 0.03 | 0.13 | 0.03 | 0.05 | 0.10 |
| UGC 7880 | 12.14 ± 0.03 | 0.91 ± 0.01 | 1.39 ± 0.01 | 3.24 ± 0.04 | 0.12 | 0.03 | 0.05 | 0.09 |
| UGC 8675 | 12.50 ± 0.03 | 0.80 ± 0.02 | 1.31 ± 0.02 | 3.20 ± 0.09 | 0.05 | 0.01 | 0.02 | 0.05 |
| UGC 11178 | 13.71 ± 0.06 | 0.89 ± 0.01 | 1.27 ± 0.01 | 3.68 ± 0.04 | 0.70 | 0.16 | 0.27 | 0.51 |
| UGC 11356 | 12.29 ± 0.07 | 0.95 ± 0.01 | 1.53 ± 0.01 | 3.52 ± 0.04 | 0.41 | 0.09 | 0.16 | 0.31 |
| UGC 11781 | 14.23 ± 0.07 | 1.18 ± 0.01 | 1.87 ± 0.01 | 3.86 ± 0.03 | 1.12 | 0.26 | 0.43 | 0.82 |
| UGC 11972 | 13.90 ± 0.06 | 1.14 ± 0.01 | 1.82 ± 0.01 | 3.79 ± 0.02 | 0.76 | 0.17 | 0.29 | 0.56 |
| UGC 12443 | 13.94 ± 0.04 | 0.99 ± 0.01 | 1.52 ± 0.01 | 3.36 ± 0.05 | 0.52 | 0.12 | 0.21 | 0.42 |
| UGC 12655 | 14.09 ± 0.05 | 0.93 ± 0.01 | 1.53 ± 0.01 | 3.50 ± 0.04 | 0.32 | 0.07 | 0.13 | 0.27 |

Note.—Col. (2) gives the measured uncorrected total *B* magnitude, cols. (3)–(5) give the measured *B*−*V*, *B*−*R*, and *V*−*K*′ color indexes, and cols. (6)–(9) give the combination of Galactic foreground extinction and *K* correction.

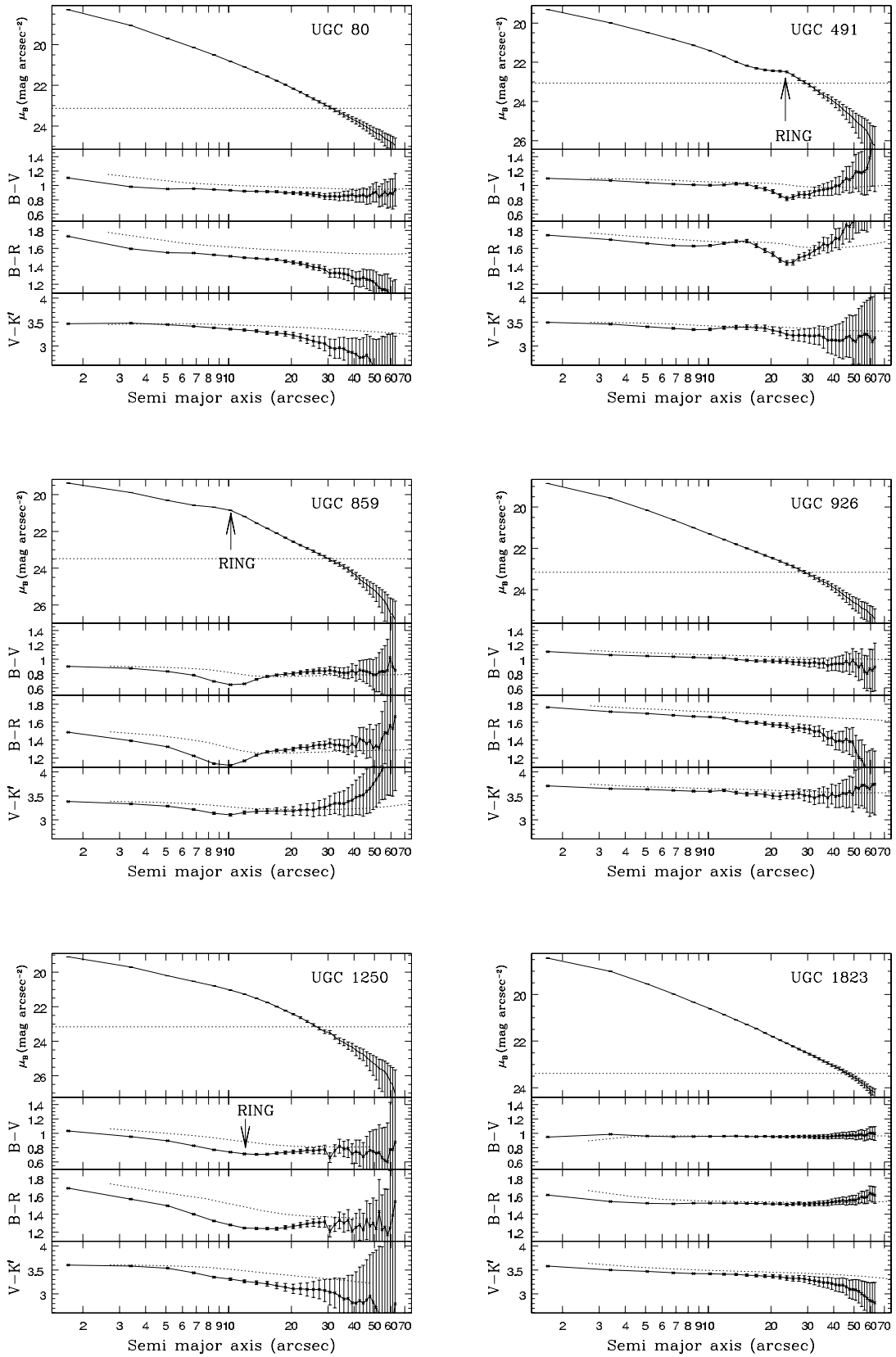


FIG. 2.—Surface brightness and color profiles along the major axis of the sample galaxies. For each galaxy, *B*-band surface brightness and the $B-V$, $B-R$, and $V-K'$ color profiles (*solid lines*) are given in separate panels. The integrated color of the galaxy in successive elliptical apertures is shown by the dotted curves. The galaxy *B*-band intensity corresponding to 10% of the sky brightness (or equivalently an error of 0.1 mag arcsec$^{-2}$) is indicated by the dotted line in the top panel. The error bars on the surface brightness profiles correspond to 1% error in the estimation of the sky background. Error bars on the color profiles are estimated by quadratically adding the uncorrelated part of the errors on the two magnitudes that contribute to the color.

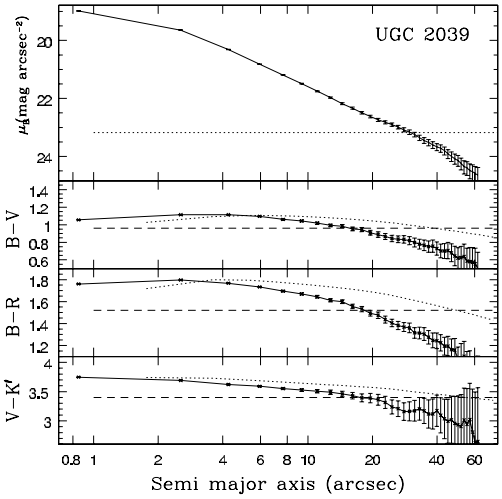


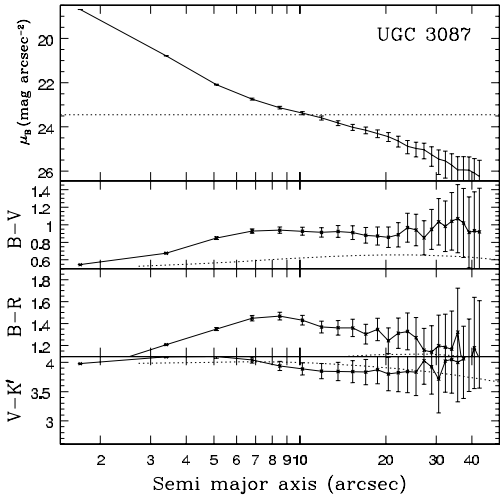


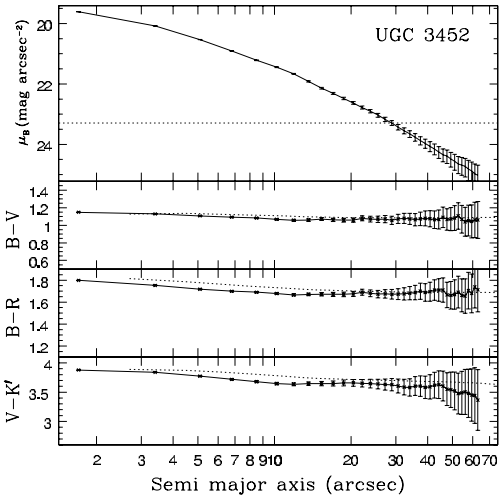


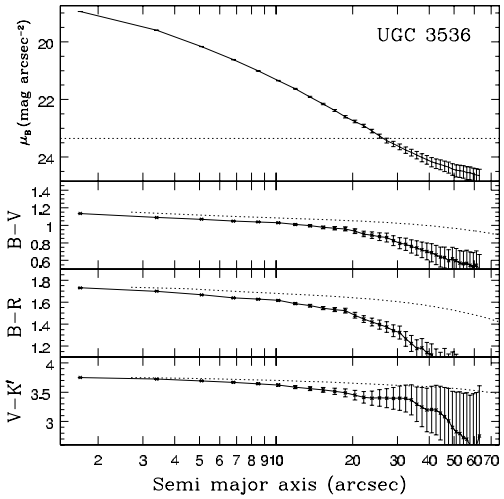


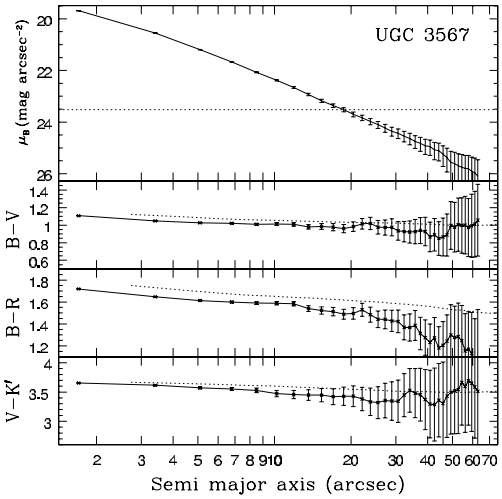


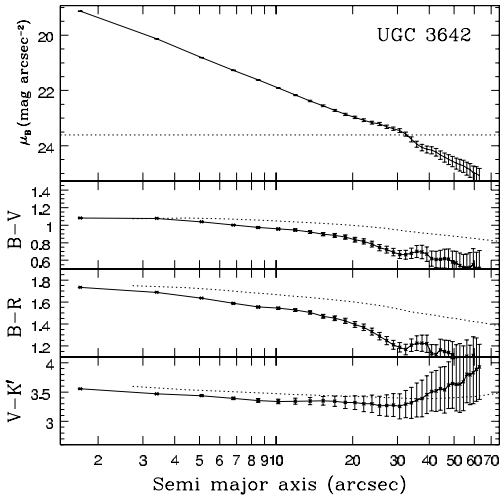


FIG. 2.—*Continued*

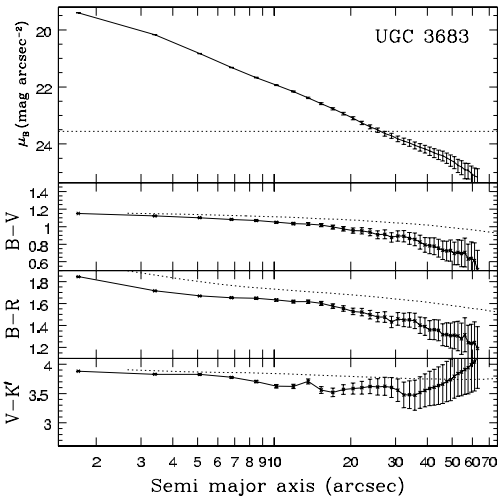


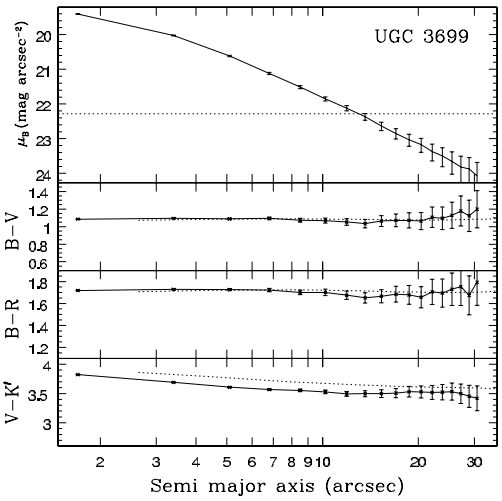


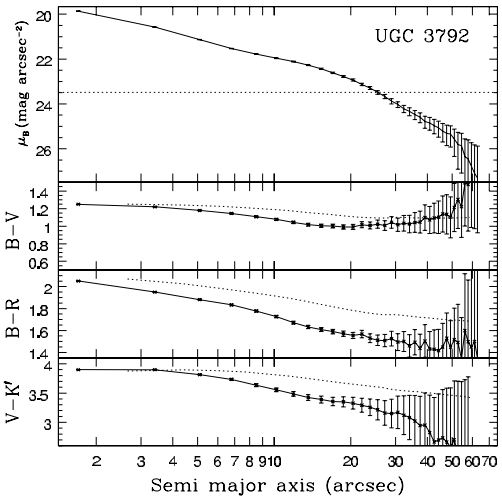


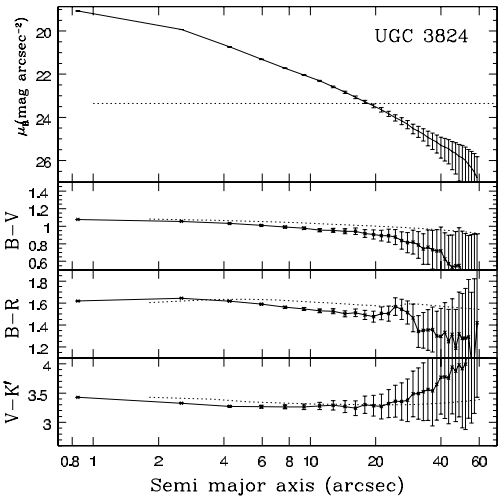


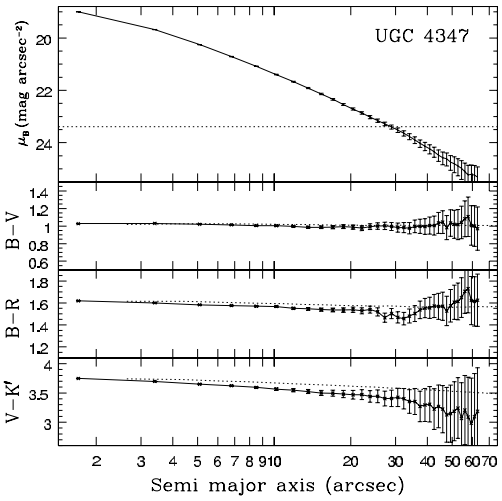


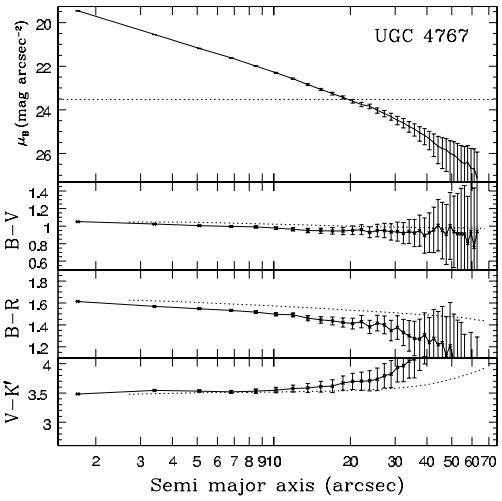


FIG. 2.—*Continued*

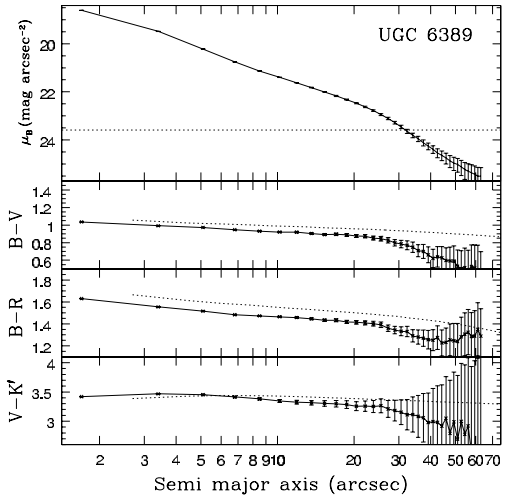


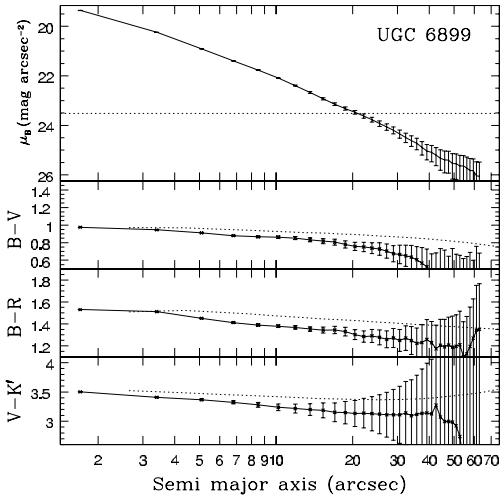


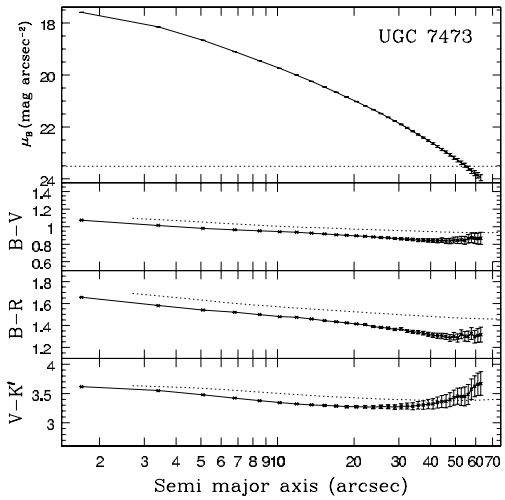


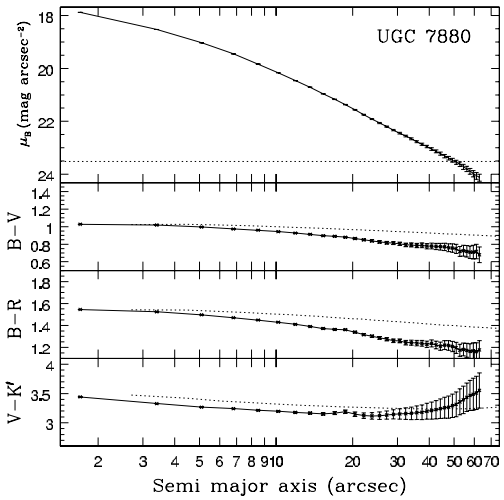


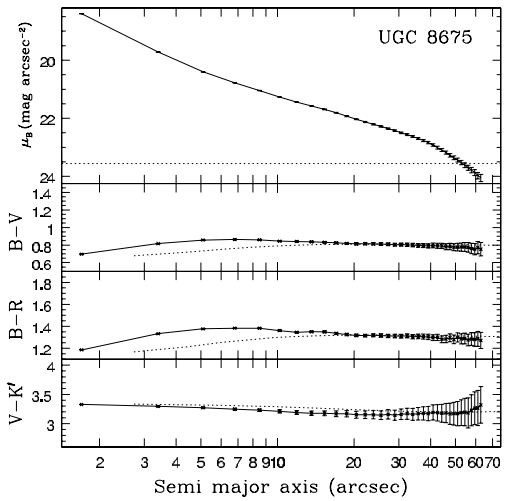


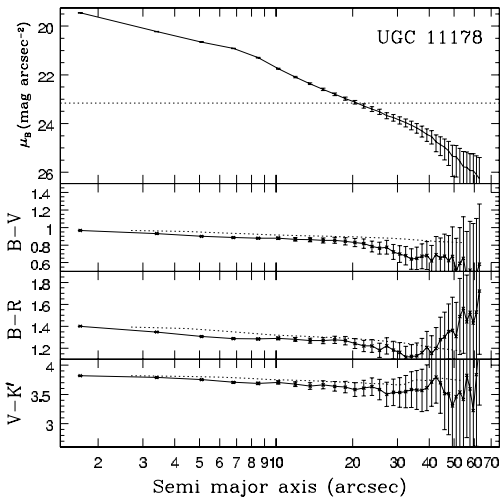


FIG. 2.—*Continued*

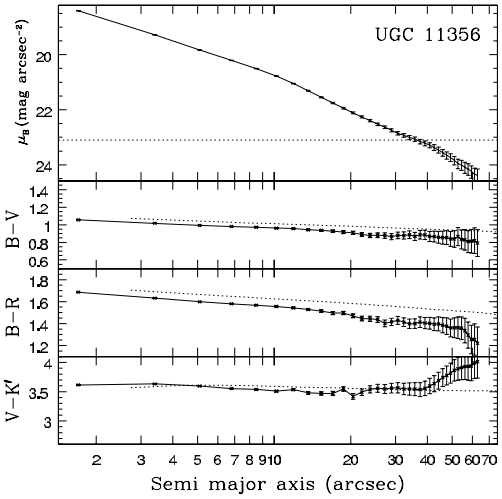


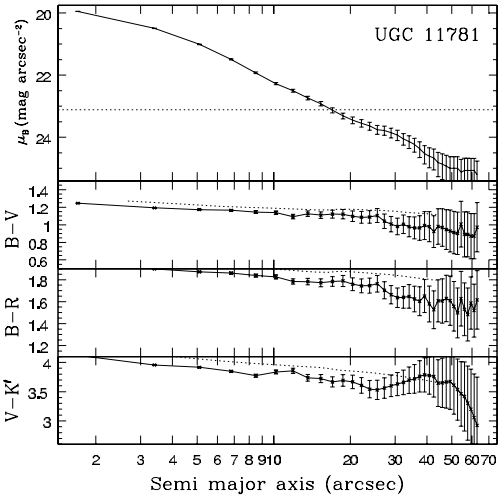


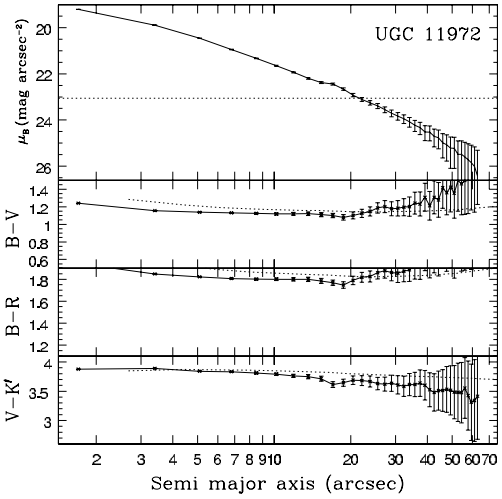


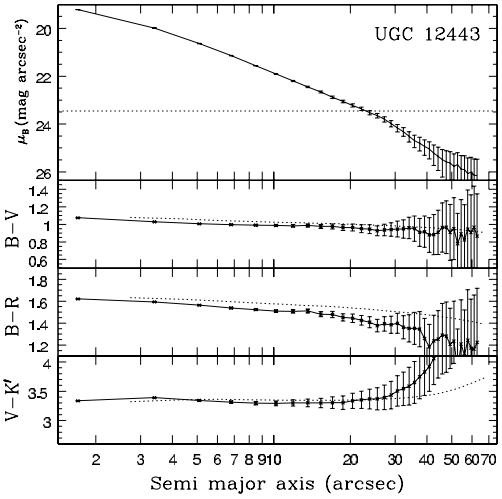


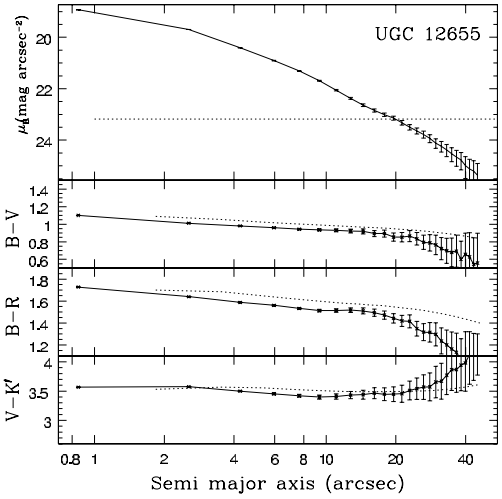


FIG. 2.—*Continued*

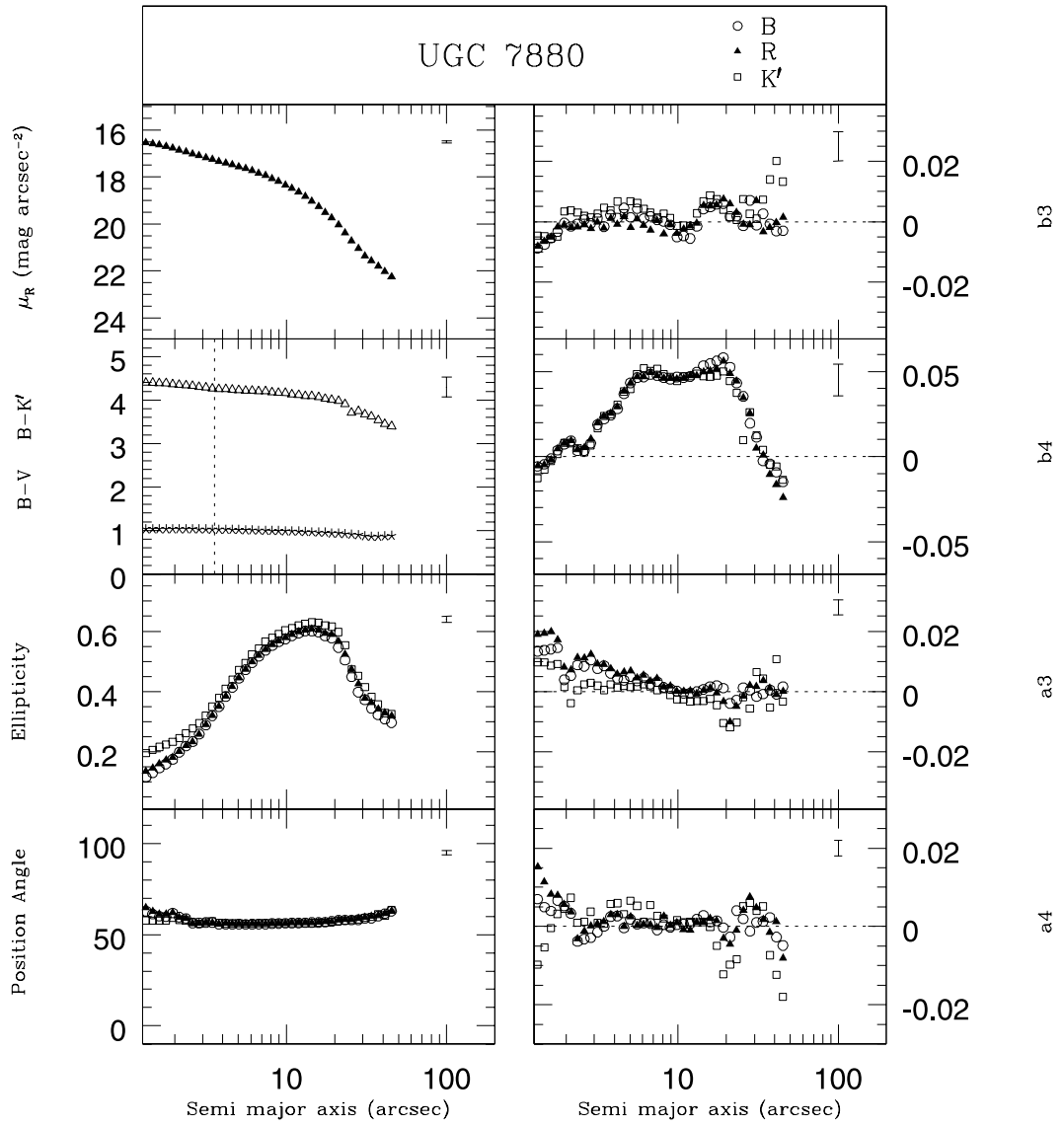


FIG. 3.—Isophotal profiles for the galaxy UGC 7880.

3 times the error in the sky background. Stars, bad pixels, etc., were identified in the first round of the fitting procedure and masked in the next run. All the parameters, including the center of the ellipse, were allowed to vary during the fitting. Variation in ellipse center was found to be small ($\sim$1.″2), which provides a check on the accuracy of the sky subtraction. We repeated the fitting process with different modes of sampling and different starting major-axis lengths to check the stability of the extracted parameters.

The fitting procedure provides the mean intensity (surface brightness) and the ellipticity and position angle of the major axis of the best-fit ellipse, as a function of the semimajor-axis length. The $B$-band surface brightness profile and the $B-V$, $B-R$, and $V-K'$ color profiles are shown for all the galaxies in Figure 2. The profiles of the ellipticity, position angle, and the Fourier coefficients $a_3$, $a_4$, $b_3$, and $b_4$ in the $B$, $R$, and $K'$ bands for one galaxy (UGC 7880) are shown in Figure 3.[3]

Color measurements of galaxies involving frames with different seeing FWHM can lead to errors at small radii and, in particular, within the seeing disk, which has to be approached for measuring nuclear colors. These errors have been discussed by Franx et al. (1989), Peletier et al. (1990a), and Goudfrooij et al. (1994), who have derived a cutoff radius for color profiles and discarded colors measured inside this limit, which is usually 2 $\times$ FWHM. Idiart et al. (2002) used a method of equalization of the FWHMs to reduce error due to different seeing FWHM, but this method is feasible only if the frames involved in color measurement are observed in quick succession. For our observations the seeing FWHM was nearly the same for the optical $B$, $V$, and $R$ bands but significantly better in $K'$, as indicated by Table 2. We have therefore degraded the $K'$ images to the mean FWHM of the optical-band images for each galaxy. The $V-K'$ color profiles shown in Figure 2 were obtained using the degraded $K'$-band images.

### 3.3. *Integrated Magnitudes*

In this work we obtain the total magnitude of each galaxy in all bands by integrating the light within the isophote corresponding

[3] Tables and plots of surface brightness and color profiles, as well as the profiles of the ellipticity, position angle, and Fourier coefficients $a_3$, $a_4$, $b_3$, and $b_4$ in the $B$, $R$, and $K'$ bands, are available for all the galaxies in the sample at http://iucaa.ernet.in/~sudhan/s0_1.html.

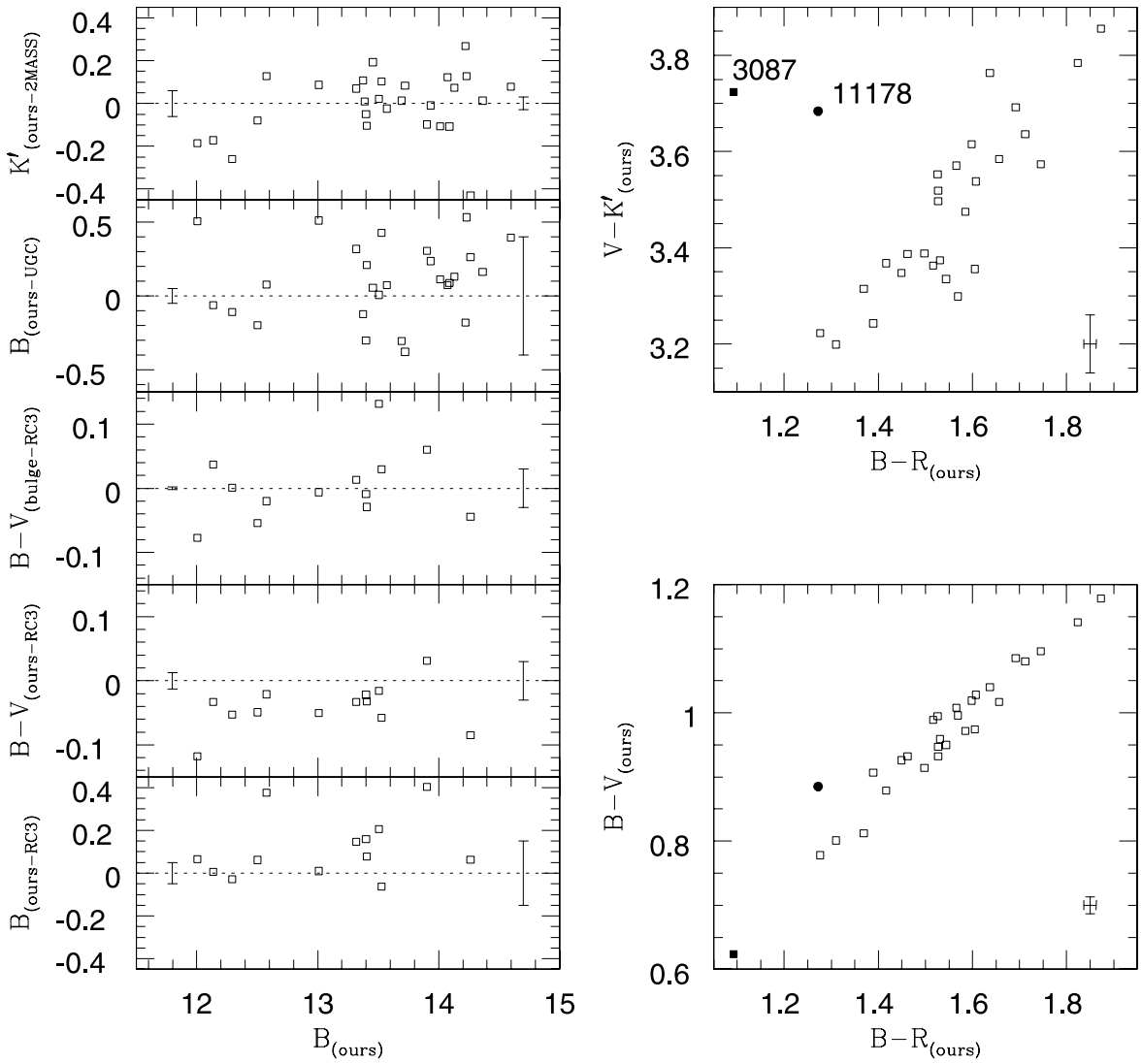


FIG. 4.—Comparison of our photometry with that in the literature. *Left*: From bottom to top, the difference between our $B$ and that of the RC3, our $B-V$ and that of the RC3, our *bulge* $B-V$ and that of the RC3, our $B$ and that of the UGC, and our $K'$ and that from 2MASS, plotted against our $B$ magnitude. Error bars on our data (*at left*) and the literature data (*at right*) are plotted on the zero-difference line. *Right*: Color vs. color plots from our data. Typical error bars are indicated in the lower right of each panel.

to $\mu_B = 25$ mag arcsec$^{-2}$ in each band. To obtain the $B-V$, $B-R$, and $V-K'$ colors, however, we integrate out only to the radius at which the error in $\mu_B$ is 0.1 mag arcsec$^{-2}$ (the radius where the dotted horizontal line intersects the $\mu_B$ profile in Fig. 2). The colors obtained in this manner are consistent with those obtained using total magnitude as defined above, within the estimated errors. However, the errors in integrated colors obtained in this manner are substantially lower (typically 0.01 vs. 0.04 in $B-V$, 0.01 vs. 0.04 in $B-R$, and 0.05 vs. 0.12 in $V-K'$). We also obtain total $K'$ magnitudes measured to $\mu_{K'} = 20$ mag arcsec$^{-2}$ in order to compare with photometry from the Two Micron All Sky Survey (2MASS). The measured total $B$ magnitudes and $B-V$, $B-R$, and $V-K'$ colors, along with the estimated errors for the 29 galaxies in the sample for which we have the necessary data, are shown in Table 4. In Figure 4 (*left*), we compare our photometry with that in the literature. We have plotted (*from bottom to top*) the difference between (1, 2) our $B$ magnitude and $B-V$ color and those from the RC3 (de Vaucouleurs et al. 1991), (3) our $B$ magnitude and that from the UGC, and (4) our $K'$ magnitude measured inside the $\mu_{K'} = 20$ mag arcsec$^{-2}$ isophote and that from 2MASS, all against our $B$ magnitude. Agreement between our $B$ magnitude and that from the RC3 is within the expected errors for all except two galaxies. Our total $B-V$ colors are systematically around 0.04 mag bluer than those of the RC3. On the other hand, if we compare the $B-V$ color obtained by integrating only up to $\mu_B = 21$ mag arcsec$^{-2}$ ("bulge color"), the agreement between the colors is excellent. The agreement with our $K'$ magnitude is also reasonably good. However, it is important to note that 2MASS magnitudes correspond to $\mu_{K'} = 20$ mag arcsec$^{-2}$ and considerable flux could be outside this radius; for example, our total $K'$ magnitudes (measured inside the radius corresponding to $\mu_B = 25$ mag arcsec$^{-2}$) are systematically brighter by $\sim$0.4 mag compared with those from 2MASS. Hence, $K'$ magnitudes in the 2MASS catalog underestimate the total flux.

To check the internal consistency of our photometry, we have plotted color-color diagrams as shown in Figure 4 (*right*). In general, there is a good correlation between these independent color measurements, and except for two galaxies, UGC 3087 and UGC 11178, the estimated colors follow the sequence

TABLE 5
COLOR GRADIENTS

| Galaxy | $r_1$ (arcsec) | $r_2$ (arcsec) | $\Delta(B-V)/\Delta \log r$ | $\Delta(B-R)/\Delta \log r$ | $\Delta(V-K')/\Delta \log r$ |
|---|---|---|---|---|---|
| UGC 80 | 3.40 | 28.05 | $-0.09 \pm 0.01$ | $-0.14 \pm 0.04$ | $-0.22 \pm 0.02$ |
| UGC 491 | 3.40 | 51.00 | $-0.25 \pm 0.03$ | $-0.26 \pm 0.03$ | $-0.25 \pm 0.00$ |
| UGC 859 | ... | ... | ... | ... | ... |
| UGC 926 | 3.40 | 34.00 | $-0.21 \pm 0.01$ | $-0.24 \pm 0.01$ | $-0.23 \pm 0.02$ |
| UGC 1250 | ... | ... | ... | ... | $-0.78 \pm 0.02$ |
| UGC 1823 | 3.40 | 34.00 | $-0.01 \pm 0.00$ | $-0.02 \pm 0.01$ | $-0.20 \pm 0.01$ |
| UGC 2039 | 3.40 | 9.35 | $-0.16 \pm 0.01$ | $-0.23 \pm 0.01$ | $-0.29 \pm 0.00$ |
| UGC 3087 | ... | ... | ... | ... | ... |
| UGC 3452 | 3.40 | 9.35 | $-0.12 \pm 0.00$ | $-0.15 \pm 0.00$ | $-0.40 \pm 0.00$ |
| UGC 3536 | 3.40 | 9.35 | $-0.14 \pm 0.00$ | $-0.19 \pm 0.00$ | $-0.21 \pm 0.00$ |
| UGC 3567 | 3.40 | 9.35 | $-0.09 \pm 0.00$ | $-0.11 \pm 0.00$ | $-0.22 \pm 0.00$ |
| UGC 3642 | 3.40 | 13.60 | $-0.25 \pm 0.00$ | $-0.30 \pm 0.00$ | $-0.20 \pm 0.02$ |
| UGC 3683 | 3.40 | 13.60 | $-0.16 \pm 0.00$ | $-0.16 \pm 0.00$ | $-0.35 \pm 0.05$ |
| UGC 3699 | 3.40 | 17.00 | $-0.05 \pm 0.01$ | $-0.12 \pm 0.01$ | $-0.33 \pm 0.01$ |
| UGC 3792 | 3.40 | 17.00 | $-0.34 \pm 0.01$ | $-0.54 \pm 0.01$ | $-0.72 \pm 0.02$ |
| UGC 3824 | 3.40 | 21.25 | $-0.18 \pm 0.01$ | $-0.19 \pm 0.01$ | $-0.06 \pm 0.04$ |
| UGC 4347 | 3.40 | 22.95 | $-0.06 \pm 0.00$ | $-0.09 \pm 0.00$ | $-0.29 \pm 0.01$ |
| UGC 4767 | 3.40 | 18.70 | $-0.12 \pm 0.01$ | $-0.21 \pm 0.01$ | $+0.12 \pm 0.02$ |
| UGC 6389 | 3.40 | 22.95 | $-0.15 \pm 0.00$ | $-0.23 \pm 0.01$ | $-0.27 \pm 0.01$ |
| UGC 6899 | 3.40 | 17.85 | $-0.19 \pm 0.01$ | $-0.20 \pm 0.01$ | $-0.23 \pm 0.01$ |
| UGC 7473 | 3.40 | 17.00 | $-0.14 \pm 0.00$ | $-0.21 \pm 0.00$ | $-0.42 \pm 0.01$ |
| UGC 7880 | 3.40 | 16.15 | $-0.18 \pm 0.01$ | $-0.23 \pm 0.01$ | $-0.26 \pm 0.01$ |
| UGC 8675 | 5.95 | 53.55 | $-0.09 \pm 0.00$ | $-0.11 \pm 0.01$ | $-0.19 \pm 0.01$ |
| UGC 11178 | 3.40 | 17.85 | $-0.10 \pm 0.01$ | $-0.17 \pm 0.01$ | $-0.29 \pm 0.02$ |
| UGC 11356 | 3.40 | 21.25 | $-0.13 \pm 0.01$ | $-0.19 \pm 0.01$ | $-0.24 \pm 0.01$ |
| UGC 11781 | 3.40 | 8.50 | $-0.12 \pm 0.00$ | $-0.15 \pm 0.00$ | $-0.45 \pm 0.02$ |
| UGC 11972 | 3.40 | 19.55 | $-0.08 \pm 0.01$ | $-0.11 \pm 0.01$ | $-0.25 \pm 0.01$ |
| UGC 12443 | 3.40 | 14.45 | $-0.10 \pm 0.00$ | $-0.18 \pm 0.01$ | $-0.16 \pm 0.01$ |
| UGC 12655 | 3.40 | 14.45 | $-0.17 \pm 0.00$ | $-0.24 \pm 0.01$ | $-0.29 \pm 0.01$ |

expected for early-type galaxies. Among these, UGC 3087 is clearly outside the 3 $\sigma$ error estimation in all the three colors. This galaxy is known to harbor an active galactic nucleus, which clearly affects the color profiles in Figure 2. Hence its colors are expected to depart significantly from the general correlation. UGC 11178, though, is within the 2 $\sigma$ error bar and is curious because it stands out in the plots, which are completely independent measurements. Further photometry would be required to understand the nature of this object. We exclude these two galaxies from further analysis.

### 3.4. *Dust*

We have used optical and $K'$-band data to study the spatial distribution of dust. We have generated extinction maps in magnitude, $A_\lambda = -2.5 \log (I_{\lambda,\mathrm{obs}}/I_{\lambda,\mathrm{model}})$, where $I_{\lambda,\mathrm{obs}}$ is the observed image in the same band and $I_{\lambda,\mathrm{model}}$ is a smoothed version of this image, obtained using the best-fit ellipse parameters. Extinction maps are particularly helpful in identifying nonaxisymmetric structure. Color maps too are of help in identifying features with wavelength-dependent intensity. We have noticed from the color and extinction maps that the lenticular galaxies UGC 3178, 3536, 3792, 4347, 7473, and 7880 show clear evidence for the presence of dust in the form of lanes or patches. In all these cases there are differences in the ellipticity and position angle profiles, as well as in the higher order Fourier coefficient profiles, in the different bands. This indicates that such differences could be used as indicators of the possible presence of dust, even when the dust is not otherwise discernible (see, e.g., Peletier et al. 1990a; Goudfrooij et al. 1994). The lenticular galaxy UGC 3792 has a very prominent dust lane along the major axis (see the Appendix for details). We will present elsewhere a detailed study of the dust in our sample of galaxies.

## 4. COLOR GRADIENTS

It is the usual practice to parameterize the color gradient over the galaxy as the slope $\Delta(B-V)/\Delta \log r$, which is evaluated by making a straight-line fit between an inner and an outer radius to the color profiles. The inner cutoff limit ($r_1$) is taken to be $\sim$1.5 times the seeing FWHM (Peletier et al. 1990a), so that seeing effects are lessened. The outer limit ($r_2$) is taken to be the point along the major axis at which the error on the mean surface brightness of the fitted ellipse reaches 0.1 mag arcsec$^{-2}$. It can be seen from Figure 2 that plots of color against the logarithm of the semimajor axis for most of our sample galaxies have a reasonably linear form between the inner and outer cutoffs. There are some cases (UGC 859, 1250, and 3087) in which the color profiles are nonlinear between $r_1$ and $r_2$ because of the presence of a strong ring (UGC 859, UGC 1250) or an active galactic nucleus (UGC 3087), which makes reliable estimation of the color gradient is difficult. The $B-V$, $B-R$, and $V-K'$ color gradients for our galaxies are given in Table 5.

The colors of the galaxies in our sample become bluer outward, in keeping with the trend observed in elliptical galaxies. The only exception to this is the positive gradient in the $V-K'$ color of the galaxy UGC 4767. After excluding UGC 3792 (which has a prominent dust lane), the mean logarithmic gradients in the $B-V$, $B-R$, and $V-K'$ colors are $-0.13 \pm 0.06$, $-0.18 \pm 0.06$, and $-0.25 \pm 0.11$ mag dex$^{-1}$ in radius, respectively. A comparison of our mean color gradients with corresponding values from the literature for elliptical galaxies and

TABLE 6
Comparison of Color Gradients

| Sample | $\Delta(B-V)/\Delta \log r$ | $\Delta(B-R)/\Delta \log r$ | $\Delta(V-K')/\Delta \log r$ |
|---|---|---|---|
| This paper | $-0.13 \pm 0.06$ (25) | $-0.18 \pm 0.06$ (25) | $-0.25 \pm 0.11$ (25) |
| Elliptical galaxies[a] | $-0.04 \pm 0.01$ (12) | $-0.09 \pm 0.02$ (30) | $-0.16 \pm 0.19$ (12) |
| Bulges of disk galaxies[b] | ... | $-0.19 \pm 0.16$ (30) | ... |

Note.—The number of galaxies used to obtain the listed mean values are indicated in parentheses. See § 4 for details.
[a] Peletier et al. 1990a, 1990b.
[b] Peletier & Balcells 1997.

the bulges of early-type spirals is given in Table 6. The color gradients are more negative for lenticular than for the elliptical galaxies, while the $B-R$ gradient for lenticular galaxies is less negative than the corresponding gradient for bulges of early-type spirals. Our steeper color gradients could imply that the metallicity gradients are stronger in lenticular galaxies or that there is more recent star formation in the outer parts of lenticulars as compared with those of elliptical galaxies. Bothun & Gregg (1990) reported significant differences in the colors of bulges and disks in lenticular galaxies, which they interpret as being due to an age difference, and not metallicity difference, between the bulge and disk components. The large rms error in the mean color gradient of our sample could be due to the different colors of the bulge and disk components and varying proportion of these in different lenticular galaxies.

Correlations between different color gradients have been noted by various authors (Peletier et al. 1990a, 1990b; Idiart et al. 2002) and have been used to derive information about the physical processes in galaxies. Such correlations are displayed in Figure 5 for our sample. A clear correlation is seen between $B-V$ and $B-R$ gradients, with correlation coefficient 0.90 at a significance level better than 99.99%. A correlation between $B-V$ and $B-R$ gradients has been noted for a sample of elliptical galaxies by Peletier et al. (1990a, 1990b). From their data we obtain a correlation coefficient of 0.97 at a significance level better than 99.99%. The plot of $V-K'$ against $B-V$ gradients shows large scatter, and we do not see any correlation of the type reported by Peletier et al. (1990b), but it should be noted that they used only 13 galaxies to derive the correlation. It is necessary to investigate how the separate bulge and disk color gradients affect the total color gradients and, hence, the correlation between them. We will address these issues in the future using a bulge-disk decomposition technique that will allow us to study the color distribution in these components separately.

## 5. CONCLUSIONS

We have presented detailed multicolor surface photometry performed with a CCD in the $B$, $V$, and $R$ bands and a NICMOS3 detector in the $K'$ band, for a sample of 34 lenticular galaxies from the Uppsala General Catalogue. The galaxies were chosen in an unbiased fashion from a subset of UGC lenticular galaxies, as explained in § 2. We have obtained total integrated magnitudes and colors for all the galaxies using elliptical annuli from surface photometry, and we find that these are in good agreement with values from the RC3. Using isophotal analysis, we have obtained radial profiles of the surface brightness, ellipticity, position angle, and higher order Fourier coefficients in all the bands. The profiles in the different bands are consistent with each other, and any differences can be attributed to the presence of dust and other features that produce wavelength-dependent effects. We have used the surface brightness profiles to obtain color profiles, and logarithmic color gradients, and find that the gradients are negative, indicating that the colors of lenticular galaxies become redder toward the center, as is the case with elliptical galaxies. We have shown that there is a good correlation between $B-V$ and $B-R$ color gradients for lenticular galaxies. Numerical profiles of all parameters that we have obtained from the isophotal analysis, along with the color images, are available online.[4]

[4] At http://www.iucaa.ernet.in/~sudhan/s0_1.html.

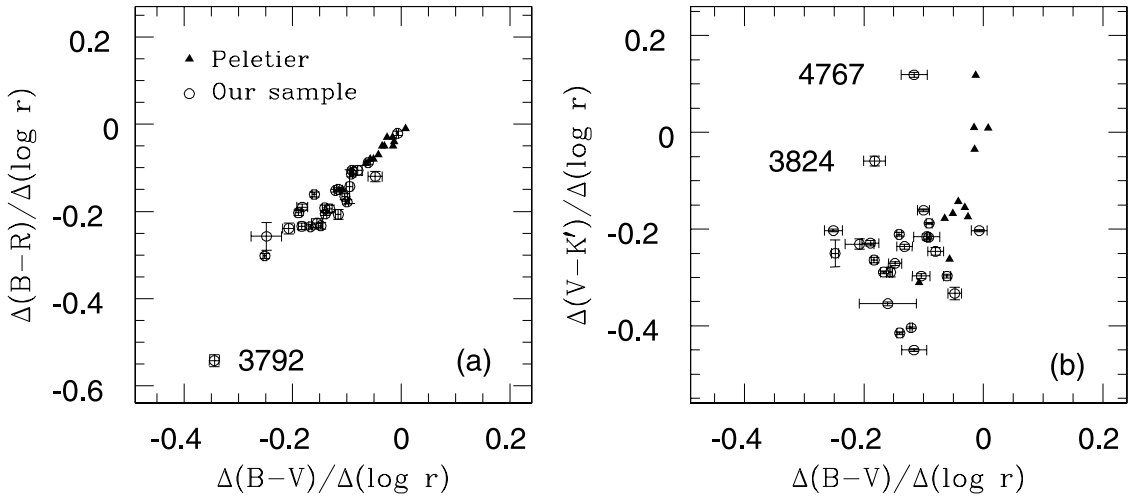


Fig. 5.—Correlation between different color gradients. The gradients for our sample and the sample of elliptical galaxies of Peletier et al. (1990a, 1990b) are shown with different symbols as indicated in (*a*).

Our intention in obtaining the multiband data on lenticular galaxies has been to study in detail these objects as a class, and to compare their properties with those of elliptical and early-type spiral galaxies. An important aspect of this study will be the decomposition of the lenticular galaxies into bulge and disk components and comparison of these separately with the bulges and disks in other types of galaxies where these components occur with varying degrees of prominence. We will use the results of the decomposition in a multiband study of the fundamental and photometric planes for lenticular galaxies. We will also make a detailed study of the distribution of dust in lenticular galaxies, particularly in those objects from our sample where there are prominent dust features and where we have multiband data at optical as well as near-infrared wavelengths.

The staff at OAGH and SPM are gratefully acknowledged for their help during the observations. S. B. and S. K. P. thank IUCAA for hospitality and the use of facilities without which this work could not have been done, and for providing funds for observations. A. K. K. and S. B. thank the Instituto Nacional de Astrofísica, Óptica y Electrónica for hospitality provided during their visits. We also thank the anonymous referee for several useful comments, which helped to improve the original manuscript. This research has made use of the NASA/IPAC Extragalactic Database (NED), which is operated by the Jet Propulsion Laboratory, California Institute of Technology, under contract with the National Aeronautics and Space Administration. This work was supported in part by CONACyT (Mexico) grant 39714-F.

## APPENDIX

In this appendix, we discuss structural properties of each galaxy whenever isophotes in one or more bands depart from a smooth ellipse. The discussions are focused on any disagreement in the morphological classification in the UGC and RC3, presence of a dust lane, change of ellipse-fit parameters ($b_4$, P.A., or ellipticity), existence of any ring, and evidence of nuclear activity. Published information on any of these issues, if available, is noted. In total, 12 galaxies (UGC 926, 1823, 3452, 3567, 3683, 3699, 3824, 6013, 6389, 6899, 11972, and 12443) are smooth lenticular galaxies without any identifiable features in the direct images, the surface brightness profiles, or the color or extinction maps. Comments for the remaining galaxies follow.

**UGC 80**: This is a barred lenticular galaxy with a very faint interacting companion. The faint bar is almost perpendicular to the galaxy major axis and is clearly evident in the isophotal profile. The $b_4$ profile is indicative of a disky shape over the entire major-axis range explored. The ellipticity and position angle profiles show an abrupt change at $r \simeq 5''$, where there is also a kink in the brightness profile. The $B-R$ color map of the galaxy shows a red feature near the center.

**UGC 491**: This is the brightest galaxy in a small group with NGC 258 and NGC 260. This galaxy is classified as S0 in the UGC and SA(r) in the RC3. In the optical images it indeed shows a ring, which is also evident in the $B-R$ and $B-K'$ color maps. Ellipticity and position angle profiles show a change at $r \sim 21\farcs5$, which may be due to the presence of the ring.

**UGC 859**: This galaxy shows an internal ring, but it is classified as S0 in the UGC. The $B-R$ and $B-K'$ color maps of the galaxy show the ring as an inhomogeneous structure. A low surface brightness disk with some luminous spiral structure exists outside the ring. UGC 859 has been detected by *IRAS* and has flux densities of $1160 \pm 33$ mJy at 60 $\mu$m and $870 \pm 319$ mJy at 100 $\mu$m (Knapp et al. 1989). The $b_4$ coefficient is disky toward the outer region.

**UGC 1250**: While this galaxy is classified as S0, the $B-R$ color map of the galaxy shows a very clear but distorted ring, just around the bulge. H$\alpha$ + [N II] observations by Pogge & Eskridge (1993) show copious H II regions across the disk. The $b_4$ profile is disky at all major-axis lengths, with the coefficient being larger in the inner region of the galaxy.

**UGC 2039**: UGC 2039 is paired with UGC 2049. There is a rise in the ellipticity from 0.1 to 0.5 toward the outer region. The $b_4$ coefficient is disky in the outer region, which suggests the presence of a significant disk. The galaxy has been detected by *IRAS* at 60 and 100 $\mu$m.

**UGC 3087**: Previous studies of UGC 3087 have mainly concentrated on its nuclear activity. It is a strong radio source (3C 120), and the optical spectrum suggests a Seyfert 1 nucleus (Tadhunter et al. 1993). It has a faint optical jet in the same apparent direction as the radio jet. The optical jet is clearly visible in our images and distorts the isophotal profiles in the inner region.

**UGC 3178**: A dust feature is clearly visible in the $B$-band extinction map of this galaxy and is also detectable from the isophotal analysis of $B$- and $K'$-band images. The $b_4$ coefficient, position angle, and ellipticity are different in $B$ and $K'$, which may be due to dust absorption in $B$. Our $V$ and $R$ band images suffer from poor signal-to-noise ratio (S/N).

**UGC 3536**: This galaxy has a significant dusty disk, and the $b_4$ coefficient is disky. The disk is also evident in the $B-V$ and $B-R$ color maps. There is a constant rise in ellipticity for semimajor-axis length less than $19\farcs5$, beyond which there is a decrease, which could be due to the disk.

**UGC 3642**: The images for this galaxy show some kind of spiral structure, but this is not evident in the extinction or color maps. The $b_4$ coefficient is positive in the outer regions.

**UGC 3792**: This galaxy is classified as S0 in the UGC but as SA0/a in the RC3, and it has no previous reported photometric study. The galaxy has a prominent dust lane along the major axis that greatly affects the various profiles. This dust lane is most prominent in the $B$ band. The $b_4$ coefficient is positive in the outer region. There is a large color gradient in $B-V$, $B-R$, and $V-K'$, presumably because of the dust. A detailed study of this galaxy in the $B$, $V$, $R$, $J$, $H$, and $K'$ bands will be presented in a forthcoming paper.

**UGC 4347**: Our $B-V$ and $B-K'$ color and extinction maps of this galaxy reveal a large dust patch near the center. The $b_4$ profile is disky throughout the observed region. Forbes & Thomson (1992) have detected possible shells in this galaxy. The extinction images in all bands show faint structures, which may be responsible for the nonzero values of the $b_4$ coefficient.

**UGC 4767**: The position angle and ellipticity profiles for this galaxy are different in the $B$, $R$, and $K'$ bands for semimajor-axis lengths of less than $5''$, which could be the result of a dust patch near the center of the galaxy. The various color maps also indicate the presence of the dust patch.

**UGC 4901**: Our $B$-band image of this galaxy has poor S/N. The color maps in $V-R$ and $V-K'$ show no features in the galaxy. The $b_4$ coefficient is positive toward the outer region, suggesting the presence of a faint disk.

**UGC 7473**: This well-studied edge-on lenticular galaxy forms a pair with NGC 4340. The surface brightness profile of this galaxy clearly indicates the presence of bulge and disk components. The $Mg_2$ line-strength profiles along the major and

minor axes of the galaxy differ dramatically and convincingly indicate the presence bulge and disk components (Fisher et al. 1996). Michard & Marchal (1993) described UGC 7473 as having a disk fully embedded in a spheroidal halo. A disk of rapidly rotating gas is present within the inner 3″; this is decoupled from the stellar component (Fisher 1997). A concentration of dust in the disk has been proposed by Michard & Poulain (2000). Our $B-R$ and $B-K'$ color and extinction maps also clearly reveal an inclined disk. The ellipticity rises from 0.2 to 0.61 over the observed region and the $b_4$ coefficient becomes significantly positive beyond 6″, which reflects the presence of a strong disk.

**UGC 7880**: This galaxy forms a pair with NGC 4635, with a separation of 1.′5. The ellipticity changes from 0.1 to 0.5 up to 10″ and decreases beyond that. The $b_4$ coefficient is positive up to the point at which the ellipticity begins to decrease. This may be due to the presence of an inner disk, the presence of which is also indicated by the $B-R$ and $B-K'$ color and extinction maps.

**UGC 7933**: This galaxy is classified as S0 in the UGC but as E1–E2 in the RC3. It forms a noninteracting pair with NGC 4670 at 5.′6 separation. The *B*-band image has poor S/N. The $b_4$ coefficient is positive toward the outer region. The color and extinction maps do not indicate any structure.

**UGC 8675**: This is a little-studied S0 galaxy hosting a Seyfert 1.5 nucleus and has been classified as an SA0 galaxy in the RC3. The isophotes of the galaxy are nearly circular, and at 5″ the ellipticity becomes 0.15, which is consistent with the values obtained by De Robertis et al. (1998) and Ferruit et al. (2000). A dust absorption pattern is seen near the nucleus in the $B-R$ and $B-K'$ color and extinction maps. Ferruit et al. (2000) have found from *Hubble Space Telescope* observations a U-shaped dust lane circling around the nucleus.

**UGC 11178**: This galaxy has no previous reported photometric study. The extinction map shows a ringlike structure in all the bands. The ellipticity abruptly changes between 5″ and 7″, which could be a result of the ringlike structure. The $b_4$ coefficient is significantly positive up to 7″. The color maps are featureless.

**UGC 11356**: This is a face-on lenticular galaxy. A faint structure is apparent in extinction images in the optical bands near the center of the galaxy, but no features are obvious in the color maps.

**UGC 11781**: This galaxy is classified as S0 in the UGC but as SAB in the RC3. The presence of a bar is clear in the direct images, as well as in the extinction images. There is a dip in the ellipticity profile at 10″, where there is a change in the position angle profile as well. The $b_4$ coefficient is positive in this region.

**UGC 12655**: The $B-R$ and $B-K'$ color and extinction maps of this galaxy show a patchy region near the center of this galaxy. The $b_4$ coefficient is positive up to 8″.

## REFERENCES


Abadi, M. G., Moore, B., & Bower, R. G. 1999, MNRAS, 308, 947
Bekki, K. 1998, ApJ, 504, 50
Bessell, M. S. 1990, PASP, 102, 1181
Bothun, G. D., & Gregg, M. D. 1990, ApJ, 350, 73
Chevalier, C., & Ilovaisky, S. A. 1991, A&AS, 90, 225
Cruz-González, I., et al. 1994, Rev. Mexicana Astron. Astrofis., 29, 197
De Robertis, M. M., Hayhoe, K., & Yee, H. K. C. 1998, ApJS, 115, 163
de Vaucouleurs, G., de Vaucouleurs, A., Corwin, H. G., Jr., Buta, R. J., Paturel, G., & Fouqué, P. 1991, Third Reference Catalogue of Bright Galaxies (Berlin: Springer)
Ferruit, P., Wilson, A. S., & Mulchaey, J. 2000, ApJS, 128, 139
Fisher, D. 1997, AJ, 113, 950
Fisher, D., Franx, M., & Illingworth, G. 1996, ApJ, 459, 110
Forbes, D. A., & Thomson, R. C. 1992, MNRAS, 254, 723 (erratum 256, 736)
Franx, M., Illingworth, G., & Heckman, T. 1989, AJ, 98, 538
Frei, Z., & Gunn, J. E. 1994, AJ, 108, 1476
Fukugita, M., Shimasaku, K., & Ichikawa, T. 1995, PASP, 107, 945
Goudfrooij, P., Hansen, L., Jørgensen, H. E., Nørgaard-Nielsen, H. U., de Jong, T., & van den Hoek, L. B. 1994, A&AS, 104, 179
Hubble, E. P. 1958, The Realm of the Nebulae (repr.; New York: Dover)
Hunt, L. K., Mannucci, F., Testi, L., Migliorini, S., Stanga, R. M., Baffa, C., Lisi, F., & Vanzi, L. 1998, AJ, 115, 2594 (erratum 119, 985 [2000])
Idiart, T. P., Michard, R., & de Freitas Pacheco, J. A. 2002, A&A, 383, 30
Jedrzejewski, R. I. 1987, MNRAS, 226, 747
Jørgensen, I., Franx, M., & Kjærgaard, P. 1992, A&AS, 95, 489
———. 1996, MNRAS, 280, 167
Khosroshahi, H. G., Wadadekar, Y., & Kembhavi, A. K. 2000a, ApJ, 533, 162
Khosroshahi, H. G., Wadadekar, Y., Kembhavi, A. K., & Mobasher, B. 2000b, ApJ, 531, L103
Knapp, G. R., Guhathakurta, P., Kim, D.-W., & Jura, M. 1989, ApJS, 70, 329
Landolt, A. U. 1992, AJ, 104, 340
Michard, R., & Marchal, J. 1993, A&AS, 98, 29
Michard, R., & Poulain, P. 2000, A&AS, 141, 1
Nilson, P. 1973, Uppsala General Catalogue of Galaxies (Uppsala: Uppsala Astron. Obs.)
Peletier, R. F., & Balcells, M. 1996, AJ, 111, 2238
———. 1997, NewA, 1, 349
Peletier, R. F., Davies, R. L., Illingworth, G. D., Davis, L. E., & Cawson, M. 1990a, AJ, 100, 1091
Peletier, R. F., Valentijn, E. A., & Jameson, R. F. 1990b, A&A, 233, 62
Persson, S. E., Frogel, J. A., & Aaronson, M. 1979, ApJS, 39, 61
Pogge, R. W., & Eskridge, P. B. 1993, AJ, 106, 1405
Rieke, G. H., & Lebofsky, M. J. 1985, ApJ, 288, 618
Schlegel, D. J., Finkbeiner, D. P., & Davis, M. 1998, ApJ, 500, 525
Tadhunter, C. N., Morganti, R., di Serego Alighieri, S., Fosbury, R. A. E., & Danziger, I. J. 1993, MNRAS, 263, 999
van den Bergh, S. 1994, AJ, 107, 153 (erratum 107, 1912)
Wadadekar, Y., Robbason, B., & Kembhavi, A. K. 1999, AJ, 117, 1219